PERGAMON

International Journal of Solids and Structures 38 (2001) 8851–8868

INTERNATIONAL JOURNAL OF SOLIDS and STRUCTURES

www.elsevier.com/locate/ijsolstr

Drag experienced by a high-speed train due to excitation of ground vibrations

A.V. Metrikine [a,*], A.V. Vostrukhov [b], A.C.W.M. Vrouwenvelder [a]

[a] *Faculty of Civil Engineering and Geosciences, Delft University of Technology, P.O. Box 5048, 2600 GA Delft, The Netherlands*
[b] *Radiophysical Department, Nizhniy Novgorod State University, Pr. Gagarina 23, 603000 Nizhniy Novgorod, Russian Federation*

Received 7 June 2000

Abstract

"Visco-elastic drag" associated with excitation of ground waves by a high speed train is investigated theoretically. Railway track is modeled by a beam that overlies a visco-elastic half-space. The train loading is described by a set of constant loads that uniformly move over the beam. The visco-elastic drag is calculated as the ratio of power (energy per unit time) of the track vibrations to the velocity of the train motion. Firstly, vibrations perturbed by a single load are considered to study dependence of the "visco-elastic drag" on the velocity of the load and on the material damping in the half-space. Secondly, by studying vibrations of the system under two loads, the effect of the distance between these loads to the visco-elastic drag is analyzed. Finally, total visco-elastic drag that is experienced by a TGV train is calculated and compared to the rolling drag and the aerodynamic drag.

Keywords: Drag; Elastic waves; Moving load; High-speed train

1. Introduction

To model the dynamic response of a railway track to a high-speed train one has to account for elastic waves that the train generates in the track subsoil. This is necessary, since a modern high-speed train can travel with a velocity comparable to or even exceeding the velocity of surface waves in the ground. By moving with such a velocity the train can cause a pronounced amplification of the track response and generate powerful ground vibrations that can be perceptible at large distances from the track.

There exists a number of papers in which the dynamic response of a three-dimensional model of the track to a moving train has been studied. One of the first studies of the problem at hand was accomplished by Filippov (1961) who considered vibrations of a beam overlying an elastic half-space under a uniformly moving constant load. He showed that the beam response grows significantly as the load approaches the speed of the Rayleigh wave in the half-space. Later, Labra (1975) demonstrated that this amplification can take place at a smaller velocity if the rails are axially stressed due to the temperature extension. Recently,

* Corresponding author. Tel.: +31-15-278-4749; fax: +31-15-278-5767.
E-mail address: a.metrikine@citg.tudelft.nl (A.V. Metrikine).

0020-7683/01/$ - see front matter
PII: S0020-7683(01)00045-2

driven by a rapid development of high-speed trains, researchers have become more active in this field and published a set of papers dealing with different three-dimensional models of the track (Krylov, 1995; Dieterman and Metrikine, 1997; Grundmann et al., 1999; Metrikine and Popp, 1999; Popp et al., 1999; Sheng et al., 1999). Regardless of the model, all these papers were primarily focused on the following three aspects of the problem; on the study of the track deflections, on the investigation of the spectrum of generated ground vibrations and on the analysis of the contact forces between the train and the rails.

Undoubtedly, the aforementioned aspects are of primary importance for the railway practice. However, having understood that ground waves play a considerable role in the dynamics of high-speed tracks, one might raise the question whether these waves consume a noticeable part of the energy needed for the high-speed train motion. The reason to raise this question may be understood by analogy with supersonic planes. Indeed, it is well known that the fuel consumption of these planes is much more pronounced than that of subsonic ones. This happens because of radiation of the sound waves into the Mach cone, which forms behind the plane as it flies supersonically. A phenomenon of the same kind would arise if a high-speed train traveled with a velocity larger than the Rayleigh wave speed. In this case, the train would be accompanied by powerful surface waves propagating within a "Mach angle" the edges of which are determined by the Rayleigh wave speed (Lansing, 1966; Miklowitz, 1978). These waves might well consume a considerable energy, especially if the train speed is close to the Rayleigh wave speed.

To explore whether the energy of elastic waves generated by a high-speed train is that of any importance for the train energy consumption, we analyze a simple three-dimensional model of the railway track. This model is composed of an Euler–Bernoulli beam of a finite width and a visco-elastic half-space. Vibrations of this system are perturbed by two loads, which represent a bogie of the train. Only the constant part of the bogie loading, which is due to the gravity force, is taken into account, therefore, the loads are assumed constant and vertical. It is further assumed that the engine of the train is powerful enough to ensure the uniform motion of the loads despite the energy loss associated with the excitation of elastic waves in the ground.

The vibrational energy transmitted by the loads into the track is studied in the steady state regime in which the displacement pattern of the beam and the half-space remains undistorted in the moving reference system. It is shown that this energy may either be dissipated due to viscosity of the half-space or radiated away by elastic waves. When the loads move sub-critically (slower than the minimal phase velocity of waves in the structure, which is about the Rayleigh wave speed), this is the viscosity that consumes all the transmitted energy. In the super-critical case, along with the viscous dissipation, a significant part of the transmitted energy is consumed by elastic waves that are excited in the beam and in the half-space.

The main objective of this paper is to study the "visco-elastic drag" that the train experiences due to the energy loss on excitation of the track vibrations. To understand the significance of the visco-elastic drag, it is compared to the rolling drag and the aerodynamic drag for a TGV train that consists of two power cars and eight passenger cars. Calculations are performed for a relatively weak soil with the Rayleigh wave speed equal to 340 km/h and the material damping rate (due to the Voigt model) lying in the range $E^*/E = 0.0005$–0.004 s. It is shown that when the train moves relatively fast (>200 km/h), the aerodynamic drag is prevalent. The visco-elastic drag is the smallest one. However, it is not negligible with respect to the rolling drag, since their ratio varies from 10% to 24% as the velocity of the train is in the range 200–400 km/h.

2. Model and governing equations

We consider the steady-state response of an Euler–Bernoulli beam of a finite width $2a$ overlying a visco-elastic half-space to a set of moving loads of a constant magnitude P, see Fig. 1.

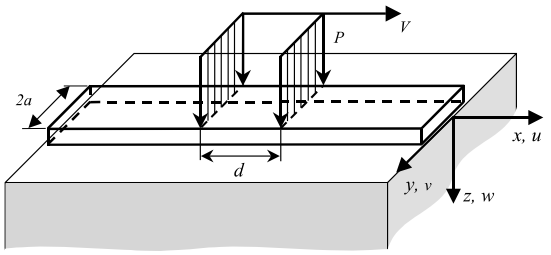

Fig. 1. Model and reference system.

The loads act upon the beam in the vertical direction, move at a fixed distance d from each other and are uniformly distributed over the beam width. The beam performs only vertical motion and its vertical displacement $w^{\text{beam}}(x,t)$ does not depend on the lateral co-ordinate y. The contact between the beam and the half-space is described approximately by assuming that the stresses at the interface are uniformly distributed over the beam width. The vertical contact is accounted for kinematically by setting the beam displacement equal to the vertical displacement of the half-space surface along the centerline of the beam. The shear contact in the x-direction is considered in the manner that is schematically depicted in Fig. 2, which presents the vertical cross-section of the system by the plane $y = 0$.

This figure shows that this contact takes place through the shear springs with stiffness per unit length K, which are assumed to be uniformly and continuously distributed beneath the beam. The end of the springs that is attached to the beam is immovable in the x-direction and the end which contacts the half-space undergoes a displacement equal to the horizontal displacement of the half-space surface along the centerline of the beam. The lateral stress σ_{yz} at the interface is neglected, for in the chosen approximation this stress does not influence the beam vertical response (Metrikine and Dieterman, 1997) and, therefore, does not affect the "visco-elastic drag".

With these assumptions, the governing equations of motion can be written as follows.

The equation of motion for the half-space

$$\hat{\mu}\Delta\boldsymbol{u} + \left(\hat{\lambda} + \hat{\mu}\right)\nabla(\nabla\boldsymbol{u}) = \rho\frac{\partial^2\boldsymbol{u}}{\partial t^2} \tag{1}$$

where $\boldsymbol{u}(x,y,z,t) = \{u(x,y,z,t), v(x,y,z,t), w(x,y,z,t)\}$ is the displacement, ρ is mass density, $\hat{\lambda} = \lambda + \lambda^*\partial/\partial t$ and $\hat{\mu} = \mu + \mu^*\partial/\partial t$ are operators that are used instead of Lamé's constants λ and μ to describe the half-space according to the Voigt phenomenological model.

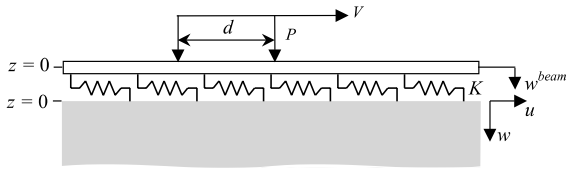

Fig. 2. Vertical cross-section $y = 0$ with magnified "beam–half-space" interface.

The boundary conditions at the surface of the half-space $z = 0$

$$\begin{aligned}
\sigma_{zz}(x,y,0,t) &= \left(A\rho_{\text{beam}}\frac{\partial^2 w^{\text{beam}}}{\partial t^2} + E_{\text{beam}}I\frac{\partial^4 w^{\text{beam}}}{\partial x^4} - P\delta(x-Vt) - P\delta(x-Vt+d)\right)\frac{H(a-|y|)}{2a},\\
\sigma_{xz}(x,y,0,t) &= Ku(x,0,0,t)\frac{H(a-|y|)}{2a},\\
\sigma_{yz}(x,y,0,t) &= 0,
\end{aligned} \tag{2}$$

where $\sigma_{zz}(x,y,z,t)$ is the normal stress, $\sigma_{xz}(x,y,z,t)$ and $\sigma_{yz}(x,y,z,t)$ are the shear stresses, $w^{\text{beam}}(x,t)$ is the vertical beam displacement, $A\rho_{\text{beam}}$ and $E_{\text{beam}}I$ are the mass per unit length and the bending stiffness of the beam, d is the distance between the loads, K is shear stiffness per unit length of the beam–half-space contact, $H(\ldots)$ is the Heaviside step function.

The compatibility condition for the vertical motion

$$w(x,0,0,t) = w^{\text{beam}}(x,t). \tag{3}$$

The goal of our study is to find the energy per unit time Q that is transmitted into the beam and the half-space by the moving loads. Having calculated this energy, one could retrieve the "visco-elastic drag" by simply dividing Q by the velocity of the loads V.

By definition, the energy per unit time that is inserted into an elastic system by a point load is equal to the scalar product of the load magnitude and the resulting velocity of the loading point. In accordance with this definition, for the model under consideration, Q reads

$$Q = P\left(\left.\frac{\partial w^{\text{beam}}}{\partial t}\right|_{x=Vt} + \left.\frac{\partial w^{\text{beam}}}{\partial t}\right|_{x=Vt-d}\right) \tag{4}$$

Expression (4) shows that to find Q one has to determine the beam displacement. This can be accomplished analytically in the manner that is described in Appendix A to give

$$w^{\text{beam}}(x,t) = \frac{P}{4\pi^2}\int_{-\infty}^{\infty}\frac{1}{\tilde{\mu}}\frac{b_{11}I_{33}-b_{21}I_{13}}{b_{11}b_{22}-b_{12}b_{21}}\left|_{\omega=k_1V}\right.\left(1+\mathrm{e}^{\mathrm{i}k_1d}\right)\mathrm{e}^{\mathrm{i}k_1(x-Vt)}\,\mathrm{d}k_1 \tag{5}$$

where

$$\begin{aligned}
b_{11}(\omega,k_1) &= \frac{K}{2\pi\tilde{\mu}}I_{11}(\omega,k_1) - 1, \qquad b_{12}(\omega,k_1) = \frac{I_{13}(\omega,k_1)}{2\pi\tilde{\mu}}D(\omega,k_1),\\
b_{21}(\omega,k_1) &= -\frac{K}{2\pi\tilde{\mu}}I_{13}(\omega,k_1), \qquad b_{22} = \frac{I_{33}(\omega,k_1)}{2\pi\tilde{\mu}}D(\omega,k_1) - 1,\\
I_{ij}(\omega,k_1) &= \int_{-\infty}^{\infty}a_{ij}(\omega,k_1,k_2)\frac{\sin k_2a}{k_2a}\,\mathrm{d}k_2, \qquad D(\omega,k_1) = -A\rho_{\text{beam}}\omega^2 + EIk_1^4
\end{aligned}$$

with expressions for a_{ij} given in Appendix A and $\tilde{\mu} = \mu - \mathrm{i}\omega\mu^*$.

Substituting expression (5) for the beam displacement into expression (4) for the energy per unit time Q, we obtain

$$Q = \frac{\mathrm{i}P^2V}{4\pi^2}\int_{-\infty}^{\infty}\frac{k_1}{\tilde{\mu}}\frac{b_{11}I_{33}-b_{21}I_{13}}{b_{11}b_{22}-b_{12}b_{21}}\left|_{\omega=k_1V}\right.\left(2+2\cos(k_1d)\right)\mathrm{d}k_1 \tag{6}$$

Expression (6) shows that the energy Q depends not only on the magnitude of the loads and on their velocity but on the distance d between the loads also. It is not surprising since the individual elastic fields generated by each load are interfering and, therefore, the energy of the total field must be influenced by the spatial shift between the individual fields.

In engineering practice, it is conventional to work with various types of drag (aerodynamic drag, rolling drag) that a train experiences while moving. Therefore, we will proceed with our analysis in terms of what we will call "visco-elastic drag" D_e that the train undergoes by perturbing vibrations of the track. By definition, this drag is given as

$$D_e = \frac{Q}{V} = \frac{iP^2}{4\pi^2} \int_{-\infty}^{\infty} \frac{k_1}{\tilde{\mu}} \frac{b_{11}I_{33} - b_{21}I_{13}}{b_{11}b_{22} - b_{12}b_{21}}\bigg|_{\omega=k_1V} (2 + 2\cos(k_1 d))\, dk_1 \tag{7}$$

The further investigation will proceed as follows. First, we will estimate a realistic value of the damping coefficient of the half-space μ^*. This is necessary, since the visco-elastic drag depends on μ^* crucially. Then, we will consider the visco-elastic drag due to a single load to clarify the effect of the damping coefficient μ^*, of the velocity V and of the shear stiffness K at the beam–half-space interface. Next, the visco-elastic drag experienced by two loads will be studied with emphasis on the effect of the distance between the loads. Employing results of this study, finally, the visco-elastic drag, the rolling drag and the aerodynamic drag will be compared for a TGV train.

3. Damping coefficient of the half-space

The decay of ground vibrations with distance from a source can be attributed to two components – geometric, or 'radiation' damping and material damping. If the source is located on the surface and the surface ground vibration are measured at a relatively large (with respect to the wavelength) distance from the source then this decay can be described by the following expression (Kim and Lee, 1998)

$$w_2 = w_1 \left(\frac{r_1}{r_2}\right)^{1/2} \exp(-\alpha(\omega)(r_2 - r_1)) \tag{8}$$

where w_1 and w_2 are the vibration amplitudes at the distance r_1 and the distance r_2 from the source, respectively, and $\alpha(\omega)$ is the material damping coefficient. The geometric damping in Eq. (8) is accounted for by the square root $\sqrt{r_1/r_2}$ that is pointing out the cylindrical character of the Rayleigh wave, which dominates at large distances from the source.

There exists a number of papers that present results of measurements of the material damping in various grounds, see Al-Hundaidi et al. (1996) and Kim and Lee (1998). As shown in these papers, in the low frequency band (below 10 Hz) the damping coefficient $\alpha(\omega)$ is in the order of 0.002–0.02 m^{-1}. The weaker and/or the softer the ground, the larger is the damping coefficient. We are especially interested in the low frequency band, for it may be shown that these are the low frequencies that primarily determine the dynamic behavior of the beam on the half-space.

The objective of this section is to determine the relation between the damping coefficient $\alpha(\omega)$ and the damping parameter μ^* that is used in our model for the half-space. To achieve this goal we consider an auxiliary problem of the steady state response of the half-space to a point harmonic load that is vertically applied to the half-space surface. It is assumed that the material damping for the half-space is small so that $\mu^*/\mu \ll 1/\omega$, where ω is the radial frequency of the load. This problem is evaluated in Appendix B. It is shown that at a large distance ($r \gg c_R/\omega$) from the load the amplitude of the surface displacement of the half-space is given as

$$|w|_{r \gg c_R/\omega} = \frac{A}{\sqrt{r}} \exp\left(-\frac{\omega^2}{2c_R} \frac{\mu^*}{\mu} r\right), \tag{9}$$

where A is an independent of r constant defined in Appendix B. Comparing expression (8) to expression (9), one may conclude that the relation between $\alpha(\omega)$ and μ^* reads

$$\alpha = \frac{\omega^2}{2c_R}\frac{\mu^*}{\mu}. \tag{10}$$

Unfortunately, we are not aware of measurements that present the dependence $\alpha(\omega)$ in the low frequency range. The only information we have at our disposal (see Kim and Lee, 1998) is related to the damping coefficient at the frequency equal to 5 Hz. Using this information and employing the relation (10), we find that for a soil with $c_R = 340$ km/h the ratio μ^*/μ lies in the following range

$$\alpha = 0.0025 - 0.02 \text{ m}^{-1} \Rightarrow \mu^*/\mu = 0.0005\text{–}0.004 \text{ s} \tag{11}$$

We will perform the further analysis assuming that the values of μ^*/μ given by Eq. (11) are realistic. It has to be beard in mind, however, that extra measurements are needed to verify the applicability of the Voigt model even in the low frequency band.

4. Visco-elastic drag for a single load

In this section, we study the visco-elastic drag faced by a single load. In this case the expression (7) for the visco-elastic drag reduces to (for example, by letting $d = 0$ and replacing P by $P/2$)

$$D_e^{\text{wheel}} = \frac{iP^2}{4\pi^2}\int_{-\infty}^{\infty}\frac{k_1}{\tilde{\mu}}\frac{b_{11}I_{33} - b_{21}I_{13}}{b_{11}b_{22} - b_{12}b_{21}}\bigg|_{\omega=k_1V} dk_1 \tag{12}$$

Evaluation of Eq. (12) was carried out numerically for the following set of the system parameters:

$$\begin{aligned} &E = 5.2\times10^7 \text{ N/m}^2, \quad \nu = 0.3, \quad \rho = 1.96\times10^3 \text{ kg/m}^3, \quad c_R = 340 \text{ km/h} \\ &A\rho_{\text{beam}} = 760 \text{ kg/m}, \quad E_{\text{beam}}I = 1.29\times10^8 \text{ N/m}^2, \quad 2a = 2.6 \text{ m}, \quad P = 10^4 \text{ kg} \end{aligned} \tag{13}$$

In this set, the half-space parameters describe a realistic soft ground, the beam parameters represent a system composed of two rails and sleepers and the load is taken to describe the wheel loading (one quarter of the passenger car weight).

Results of numerical integration of Eq. (12) are presented in Fig. 3 that show the dependence of the visco-elastic drag D_e on the velocity V of the load. Both figures present four curves that are plotted for different values of the damping coefficient μ^*, namely for $\mu_1^* = 10^3$ Ns/m^2, $\mu_2^* = 10^4$ Ns/m^2, $\mu_3^* = 0.8\times10^5$ Ns/m^2, $\mu_4^* = 10^6$ Ns/m^2. The values of μ_2^* and μ_3^* correspond to the ratios $\mu^*/\mu = 0.0005$ s and $\mu^*/\mu = 0.004$ s that, in accordance with Eq. (11), are believed to be realistic. The difference between Fig. 3a and b is that the first one is plotted for $K = 0$, i.e. in the absence of the shear contact springs, while the second presents results calculated for $K = 10^8$ N/m.

Analyzing the figures the following conclusions may be drawn:

1. For realistic values of the damping coefficient, the visco-elastic drag grows significantly as the train approaches the Rayleigh wave velocity.
2. Below the Rayleigh wave velocity ($V < c_R$), the only cause for the visco-elastic drag to occur is the material damping in the subsoil. In this range of velocities, the smaller the damping coefficient, the smaller is the visco-elastic drag.
3. At velocities higher than the Rayleigh wave velocity ($V > c_R$), the visco-elastic drag is caused both by the damping and by the so-called radiation damping that is related to the energy loss on excitation of elastic waves in the beam and the half-space. When the material damping is small, the radiation damping plays a dominant role in causing the visco-elastic drag. It is interesting to note that for $V > c_R$ the higher the

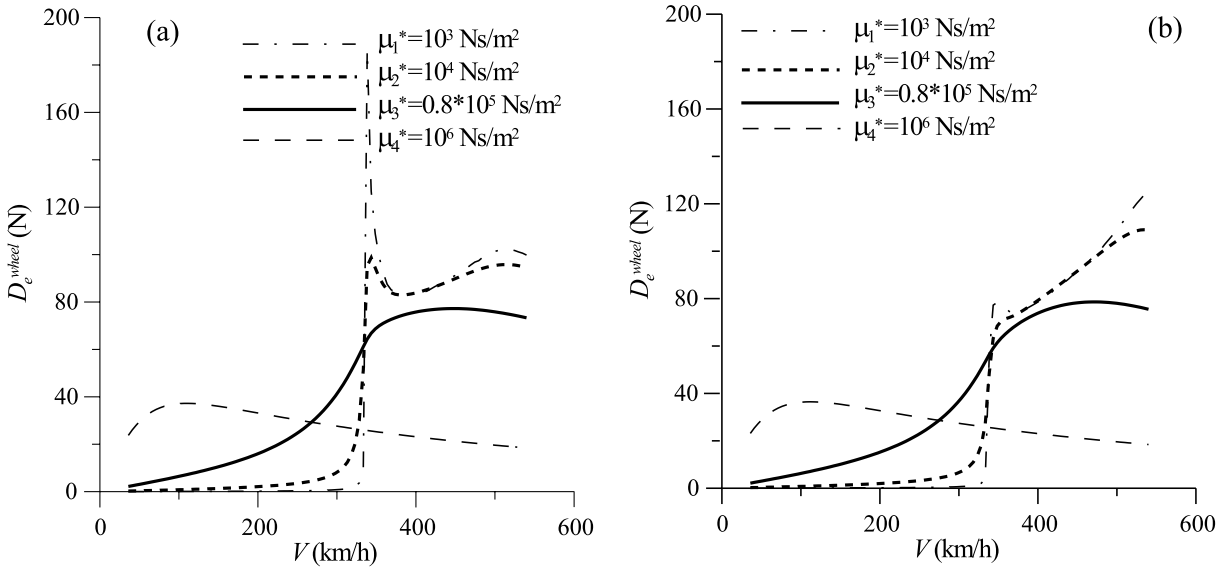

Fig. 3. Visco-elastic drag versus velocity for (a) $K = 0$, (b) $K = 10^8$ N/m.

damping coefficient, the lower is the drag. It is hard to say whether for an arbitrary velocity from the range at hand this effect would be modified if a different damping model were considered. However, for velocities close to the Rayleigh wave velocity, it is certain that introduction of any damping mechanism would reduce the drag with respect to the pure elastic case. This is because in the pure elastic case the system displacement and, consequently, the drag tend to infinity as $V \to c_R + 0$ (for $V < c_R$ the elastic drag is then zero). In a damped case the drag is always finite and, therefore, for $V \to c_R + 0$ it is always smaller than that in the pure elastic case.

4. Concerning the effect of the shear interaction between the beam and the half-space that is taken into account by the shear springs K, one can see that this effect is noticeable when the damping is relatively small and the load velocity is close to the Rayleigh wave velocity. Otherwise, the shear springs have almost no influence on the visco-elastic drag.

5. Visco-elastic drag for two loads

The final objective of this paper is to calculate the total visco-elastic drag that is experienced by a high-speed train. To accomplish this, we may not just multiply the visco-elastic drag obtained for a single wheel by the number of wheels in the train. Such an approach would give a wrong result, since every wheel is dragged not only by its own elastic field but also by elastic fields perturbed by other wheels. Mathematically, the effect of a neighbouring wheel on the visco-elastic drag is presented by $\cos(k_1 d)$ in the expression (7) for the visco-elastic drag experienced by two loads.

To explore the effect of this "cross-drag", we numerically integrate Eq. (7) by employing the parameter set (13) and $K = 10^8$ N/m. The result is shown in Fig. 4a and b. Each figure presents two curves – the solid curve corresponds to the super-critical motion with $V = 400$ km/h and the dashed curve corresponds to the sub-critical motion with $V = 200$ km/h. The figures differ due to the damping coefficient used in the

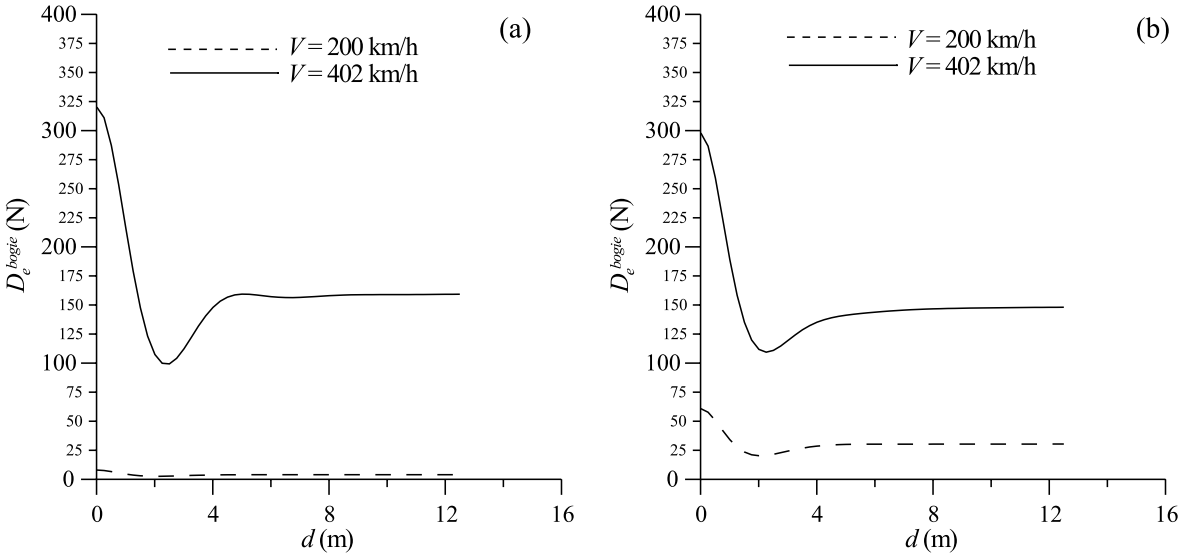

Fig. 4. Visco-elastic drag versus distance between two loads for (a) $\mu^* = 10^4$ Ns/m^2; (b) $\mu^* = 0.8 \times 10^5$ Ns/m^2.

calculations – Fig. 4a is plotted for $\mu^* = 10^4$ Ns/m^2, while Fig. 4b depicts results obtained with $\mu^* = 0.8 \times 10^5$ Ns/m^2.

The figures demonstrate the following:

1. Visco-elastic drag in the case of the super-critical motion is substantially larger than that in the case of the sub-critical motion. The difference, however, decreases when the material damping becomes larger.
2. Visco-elastic drag depends upon the distance between the loads if this distance is relatively small – $d < 5$ – 6 m. For larger distances, the drag remains unchanged and could be calculated by simple doubling of the drag calculated for the single load.
3. The dependence of the visco-elastic drag upon the distance has a minimum located approximately at $d = 2$–2.5 m. This implies that the "cross-drag" can be negative, i.e. it can push the load set forward. We would like to note that the existence of this minimum might be used in practice, for by slightly varying the bogie wheelbase one can reduce the visco-elastic drag. It should not be forgotten, however, that the optimal wheelbase depends on the soil properties and has to be found anew once the soil parameters differ from that considered in this paper.

Based upon the information retrieved from Fig. 4, we can calculate the total visco-elastic drag to the high-speed train motion. Indeed, since the distance between the bogies of a train is larger than 6 m, the contribution of each bogie may be calculated separately and then multiplied by the number of bogies on the train.

Let us consider a TGV train consisting of two power cars and eight passenger cars. We use this example, since there is an information available on the rolling drag and the aerodynamic drag that this train experiences, (see Hopkins et al., 1999). According to this paper, the weight of the power car is about 80 000 kg, the weight of the passenger car is 40 000 kg and the bogie wheelbase is 3 m. Thus, we have four "heavy bogies" with the wheel loading of 20 000 kg and sixteen "light bogies" with the wheel loading 10 000 kg. Taking the parameter set corresponding to Fig. 4a and, as an example, choosing the super-critical motion with $V = 400$ km/h, one obtains the following value for the total visco-elastic drag:

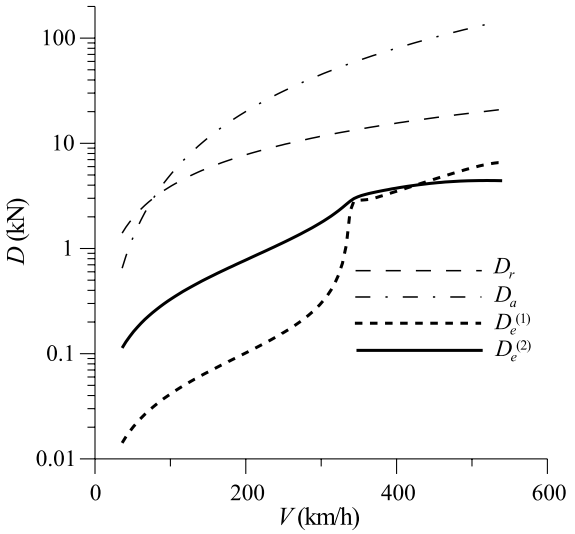

Fig. 5. Visco-elastic drag for $\mu^* = 10^4$ Ns/m^2 ($D_e^{(1)}$), visco-elastic drag for $\mu^* = 0.8 \times 10^5$ Ns/m^2 ($D_e^{(2)}$), rolling drag (D_r) and aerodynamic drag (D_a) versus velocity.

$$D_e^{\text{total}} = 4D_e^{\text{bogie}}\big|_{d=3\ \text{m}, P=200\ \text{kN}} + 16D_e^{\text{bogie}}\big|_{d=3\ \text{m}, P=100\ \text{kN}} = 4 \times 4D_e^{\text{bogie}}\big|_{d=3\ \text{m}, P=100\ \text{kN}} + 16D_e^{\text{bogie}}\big|_{d=3\ \text{m}, P=100\ \text{kN}} = 32D_e^{\text{bogie}}\big|_{d=3\ \text{m}, P=100\ \text{kN}} \approx 32 \times 120\ \text{N} = 3.84\ \text{kN} \tag{14}$$

Evaluating Eq. (14), we have taken into account that the visco-elastic drag is proportional to P^2 (see Eq. (7)) so that $D_e^{\text{bogie}}\big|_{d=3\ \text{m}, P=200\ \text{kN}} = 4 \times D_e^{\text{bogie}}\big|_{d=3\ \text{m}, P=100\ \text{kN}}$. Additionally we have used Fig. 4a which shows that $D_e^{\text{bogie}}\big|_{d=3\ \text{m}, P=100\ \text{kN}}$ is approximately equal to 120 N.

In the same manner the total drag may be calculated for any value of μ^* and V. The result of this calculation is depicted in Fig. 5 that shows the velocity dependence of the total visco-elastic drag for $\mu^* = 10^4$ Ns/m^2 (bold dashed line) and for $\mu^* = 0.8 \times 10^5$ Ns/m^2 (bold solid line). For comparison, the aerodynamic drag, and the rolling drag are plotted in accordance with results presented in Hopkins et al. (1999).

Fig. 5 shows that the largest drag that the train experiences while moving with a relatively high velocity (>200 km/h) is the aerodynamic drag. The rolling drag and the visco-elastic drag are much smaller. For example, if the train moved with $V = 400$ km/h, then the aerodynamic drag would be about 80 kN, the rolling drag would be in the order of 16 kN and the visco-elastic drag would be 3.84 kN. Thus, as one can see, the visco-elastic drag at this velocity is about 24% of the rolling drag and about 5% of the aerodynamic drag. In the case of sub-critical motion with $V = 200$ km/h, these values would respectively turn into 1.5% and 0.5% for $\mu^* = 10^4$ Ns/m^2 and into 10% and 3.8% for $\mu^* = 0.8 \times 10^5$ Ns/m^2.

Thus, the visco-elastic drag is very small with respect to the aerodynamic drag. With respect to the rolling drag, the visco-elastic drag is not that small and the higher the velocity of the train, the larger is the relative contribution of the visco-elastic drag.

6. Conclusions

In this paper, we have theoretically studied an "visco-elastic drag" to the movement of a high-speed train. This drag is associated with excitation of elastic waves in the rails and in the ground.

Consuming certain part of the train energy, these waves cause resistance – the visco-elastic drag – to the train motion.

To model railway track, a three-dimensional model has been employed composed of a visco-elastic half-space and a beam with a finite width overlying the half-space. The only constant part of the train loading has been taken into account by considering a set of constant and uniformly moving loads acting upon the beam.

The visco-elastic drag has been calculated as the ratio of power (energy per unit time) of the system vibrations to the velocity of the train motion. It has been shown that the visco-elastic drag strongly depends on the train velocity and grows considerably when the train approaches the Rayleigh wave velocity in the ground (half-space). When the train moves slower than the Rayleigh wave velocity (sub-critical motion), then the only cause for the visco-elastic drag to occur is the material damping in the half-space. The smaller the damping coefficient, the smaller is the visco-elastic drag. In the case of super-critical motion, when the train moves faster than the Rayleigh wave velocity, the visco-elastic drag is caused both by the material damping and by the so-called radiation damping that is related to the energy loss on excitation of elastic waves in the beam and the half-space. When the damping coefficient is small, the radiation damping plays a dominant role in causing the visco-elastic drag.

The visco-elastic drag experienced by a set of two loads depends on the distance between these loads. However, if this distance is large (for the model under consideration "large distance d" means $d > 6$ m), then the total drag experienced by the set of loads is equal to the sum of drags faced by the individual loads of this set. The dependence of the visco-elastic drag on the distance between the loads has a minimum that corresponds to $d = 2$–2.5 m. Existence of this minimum might be used in the railway practice, for by slightly varying the bogie wheelbase one can perceptibly reduce the visco-elastic drag.

The total visco-elastic drag experienced by a TGV train that consists of two power cars and eight passenger cars has been calculated and compared to the rolling drag and the aerodynamic drag. It has been shown that when the train moves relatively fast (>200 km/h), the aerodynamic drag is prevalent. The visco-elastic drag is the smallest one. However, it is not negligible with respect to the rolling drag, since their ratio varies from 10% to 24% as the velocity of the train is in the range 200–400 km/h.

Looking at numbers for the elastic drag, which we have obtained in this paper, one may intend to conclude that the visco-elastic drag is of minor importance for railway practice. We would not advise such a conclusion, since the model that has been considered is a very basic one and does not include into consideration many factors that should increase the visco-elastic drag. Among these factors, we can mention the sleepers, which would cause a so-called "transition radiation" of waves in the ground (Vesnitskii and Metrikine, 1996) thereby increasing the visco-elastic drag. Additionally, the pads that are usually inserted between the sleepers and the rails could consume a substantial energy since they are highly viscous. Lastly, we should not forget about possible resonance occurring should the bogie wheelbase be divisible into the wavelength of the rail vibrations.

To consider the effect of the aforementioned factors, we are planning to consider a more sophisticated model for the track (close to that considered in Metrikine and Popp (1999)) and take into account the internal degrees of freedom of the train.

Acknowledgements

The present study was partly supported by the Russian Foundation for Basic Research, grant 00-01-00344. This support is highly appreciated.

Appendix A

To analyze the system of Eqs. (1)–(3), we use the Helmholtz decomposition of the displacement vector:

$$\boldsymbol{u} = \nabla\varphi + \nabla \times \boldsymbol{\psi}, \qquad \nabla \cdot \boldsymbol{\psi} = 0. \tag{A.1}$$

In terms of the potentials φ and ψ the equations of the half-space motion read (Achenbach, 1973)

$$\hat{c}_{\mathrm{L}}^2 \nabla^2 \varphi = \frac{\partial^2 \varphi}{\partial t^2}, \qquad \hat{c}_{\mathrm{T}}^2 \nabla^2 \boldsymbol{\psi} = \frac{\partial^2 \psi}{\partial t^2} \tag{A.2}$$

with $\hat{c}_{\mathrm{L}}^2 = (\hat{\lambda} + 2\hat{\mu})/\rho, \qquad \hat{c}_{\mathrm{T}}^2 = \hat{\mu}/\rho.$

The components of the half-space displacement vector and the stresses in the half-space may be written in terms of these potentials as (Achenbach, 1973)

$$u = \frac{\partial \varphi}{\partial x} + \frac{\partial \psi_z}{\partial y} - \frac{\partial \psi_y}{\partial z}, \quad v = \frac{\partial \varphi}{\partial y} - \frac{\partial \psi_z}{\partial x} + \frac{\partial \psi_x}{\partial z}, \quad w = \frac{\partial \varphi}{\partial z} + \frac{\partial \psi_y}{\partial x} - \frac{\partial \psi_x}{\partial y}, \tag{A.3}$$

$$\sigma_{zz} = \hat{\lambda}\nabla^2\varphi + 2\hat{\mu}\left(\frac{\partial^2 \varphi}{\partial z^2} + \frac{\partial}{\partial z}\left(\frac{\partial \psi_y}{\partial x} - \frac{\partial \psi_x}{\partial y}\right)\right) \tag{A.4}$$

$$\sigma_{xz} = \hat{\mu}\left(2\frac{\partial^2 \varphi}{\partial x \partial z} + \frac{\partial}{\partial z}\left(\frac{\partial \psi_z}{\partial y} - \frac{\partial \psi_y}{\partial z}\right) + \frac{\partial}{\partial x}\left(\frac{\partial \psi_y}{\partial x} - \frac{\partial \psi_x}{\partial y}\right)\right) \tag{A.5}$$

$$\sigma_{yz} = \hat{\mu}\left(2\frac{\partial^2 \varphi}{\partial y \partial z} - \frac{\partial}{\partial z}\left(\frac{\partial \psi_z}{\partial x} - \frac{\partial \psi_x}{\partial z}\right) + \frac{\partial}{\partial y}\left(\frac{\partial \psi_y}{\partial x} - \frac{\partial \psi_x}{\partial y}\right)\right) \tag{A.6}$$

We solve the problem (1)–(3) by employing integral Fourier transforms with respect to time and the horizontal co-ordinates that are defined as

$$\begin{aligned} f(k_1,k_2,z,\omega) &= \int_{-\infty}^{\infty}\int_{-\infty}^{\infty}\int_{-\infty}^{\infty} \varphi(x,y,z,t)\exp\left(\mathrm{i}(\omega t - k_1 x - k_2 y)\right)\mathrm{d}x\,\mathrm{d}y\,\mathrm{d}t \\ \boldsymbol{g}(k_1,k_2,z,\omega) &= \int_{-\infty}^{\infty}\int_{-\infty}^{\infty}\int_{-\infty}^{\infty} \boldsymbol{\psi}(x,y,z,t)\exp\left(\mathrm{i}(\omega t - k_1 x - k_2 y)\right)\mathrm{d}x\,\mathrm{d}y\,\mathrm{d}t \\ w^{\mathrm{beam}}_{\omega,k_1}(\omega,k_1) &= \int_{-\infty}^{\infty}\int_{-\infty}^{\infty} w^{\mathrm{beam}}(x,t)\exp\left(\mathrm{i}\omega t - \mathrm{i}k_1 x\right)\mathrm{d}x\,\mathrm{d}t. \end{aligned} \tag{A.7}$$

Application of these transforms to Eqs. (A.1)–(A.3) gives the following system of equations in the Fourier domain:

1. For the half-space motion (from Eq. (A.1))

$$\begin{aligned} &\frac{\partial^2 f}{\partial z^2} + \left(\frac{\omega^2}{\tilde{c}_{\mathrm{L}}^2} - k_1^2 - k_2^2\right) f = 0 \\ &\frac{\partial^2 \boldsymbol{g}}{\partial z^2} + \left(\frac{\omega^2}{\tilde{c}_{\mathrm{T}}^2} - k_1^2 - k_2^2\right)\boldsymbol{g} = 0 \\ &\mathrm{i}k_1 g_x + \mathrm{i}k_1 g_y + \frac{\partial g_z}{\partial z} = 0 \end{aligned} \tag{A.8}$$

in which $\tilde{c}_{\mathrm{L}}^2 = c_{\mathrm{L}}^2 - \mathrm{i}\omega(\lambda^* + 2\mu^*)/\rho$, $\tilde{c}_{\mathrm{T}}^2 = c_{\mathrm{T}}^2 - \mathrm{i}\omega\mu^*/\rho$ are complex values, $c_{\mathrm{L}} = \sqrt{(\lambda + 2\mu)/\rho}$ is the velocity of the compressional waves (*P*-waves), $c_{\mathrm{T}} = \sqrt{\mu/\rho}$ is the velocity of the shear waves (*S*-waves).

2. For the boundary conditions at the surface of the half-space $z=0$ (from Eq. (2), employing Eqs. (A.4)–(A.6))

$$\begin{aligned}
&(\mu-\mathrm{i}\omega\mu^*)\left[2\mathrm{i}k_1\frac{\partial f}{\partial z}+\frac{\partial}{\partial z}\left(\mathrm{i}k_2 g_z-\frac{\partial g_y}{\partial z}\right)+\mathrm{i}k_1\left(\mathrm{i}k_1 g_y-\mathrm{i}k_2 g_x\right)\right]_{z=0}=Ku_{\omega,k_1}\frac{\sin k_2 a}{ak_2}\\
&(\mu-\mathrm{i}\omega\mu^*)\left[2\mathrm{i}k_2\frac{\partial f}{\partial z}-\frac{\partial}{\partial z}\left(\mathrm{i}k_1 g_z-\frac{\partial g_y}{\partial z}\right)+\mathrm{i}k_2\left(\mathrm{i}k_1 g_y-\mathrm{i}k_2 g_x\right)\right]_{z=0}=0\\
&\left[(\lambda-\mathrm{i}\omega\lambda^*)\left(\frac{\partial^2}{\partial z^2}-k_1^2-k_2^2\right)f+2(\mu-\mathrm{i}\omega\mu^*)\left(\frac{\partial^2 f}{\partial z^2}+\frac{\partial}{\partial z}\left(\mathrm{i}k_1 g_y-\mathrm{i}k_2 g_x\right)\right)\right]_{z=0}\\
&\qquad=\left(w^{\mathrm{beam}}_{\omega,k_1}D(\omega,k_1)-2\pi P\delta(\omega-k_1V)\left(1+\mathrm{e}^{\mathrm{i}k_1 d}\right)\right)\frac{\sin k_2 a}{k_2 a}
\end{aligned}\tag{A.9}$$

where $D(\omega,k_1)=-m\omega^2+E_{\mathrm{beam}}Ik_1^4$ is the dispersion relation for the vertical individual vibration of the beam and

$$\begin{aligned}
u_{\omega,k_1}(k_1,0,0,\omega)&=\int_{-\infty}^{\infty}\int_{-\infty}^{\infty}u(x,0,0,t)\exp\left(\mathrm{i}(\omega t-k_1x)\right)\mathrm{d}x\,\mathrm{d}t\\
w_{\omega,k_1}(k_1,0,0,\omega)&=\int_{-\infty}^{\infty}\int_{-\infty}^{\infty}w(x,0,0,t)\exp\left(\mathrm{i}(\omega t-k_1x)\right)\mathrm{d}x\,\mathrm{d}t.
\end{aligned}$$

3. For the compatibility condition (from Eq. (3))

$$w^{\mathrm{beam}}_{\omega,k_1}(\omega,k_1)=\frac{1}{2\pi}\int_{-\infty}^{\infty}w_{\omega,k_1,k_2}(k_1,k_2,0,\omega)\,\mathrm{d}k_2.\tag{A.10}$$

The general solutions of the first two equations of the system (A.8), accounting for the proper behavior for the large positive values of z, are

$$\begin{aligned}
f&=A(k_1,k_2,\omega)\exp(-zR_{\mathrm{L}})\\
\boldsymbol{g}&=\boldsymbol{B}(k_1,k_2,\omega)\exp(-zR_{\mathrm{T}})
\end{aligned}\tag{A.11}$$

with $R_{\mathrm{L,T}}=\sqrt{k_1^2+k_2^2-\omega^2/\tilde{c}^2_{\mathrm{L,T}}}$, $(\mathrm{Re}(R_{\mathrm{L,T}})>0)$.

Substituting (A.11) into the third equation of the system (A.8) and into the boundary conditions (A.9) one may obtain the following system of linear algebraic equations with respect to unknowns A and $\boldsymbol{B}$:

$$\begin{aligned}
\mathrm{i}k_1B_x+\mathrm{i}k_2B_y-R_{\mathrm{T}}B_z&=0\\
-2\mathrm{i}k_1R_{\mathrm{L}}A+k_1k_2B_x+\left(-R_{\mathrm{T}}^2-k_1^2\right)B_y+(-\mathrm{i}k_2R_{\mathrm{T}})B_z&=H_x\\
-2\mathrm{i}k_2R_{\mathrm{L}}A+\left(R_{\mathrm{T}}^2+k_1^2\right)B_x+(-k_1k_2)B_y+(-\mathrm{i}k_1R_{\mathrm{T}})B_z&=0\\
\left(2\left(k_1^2+k_2^2\right)-\frac{\omega^2}{\tilde{c}_{\mathrm{T}}^2}\right)A+2\mathrm{i}k_2R_{\mathrm{T}}B_x+(-2\mathrm{i}k_1R_{\mathrm{T}})B_y&=H_z
\end{aligned}\tag{A.12}$$

with

$$\begin{cases}
H_x=\frac{Ku_{\omega,k_1}}{(\mu-\mathrm{i}\omega\mu^*)}\frac{\sin k_2a}{k_2a}\\
H_z=\frac{1}{(\mu-\mathrm{i}\omega\mu^*)}\frac{\sin k_2a}{k_2a}\left[w^{\mathrm{beam}}_{\omega,k_1}D(\omega,k_1)-2\pi P\delta(\omega-k_1V)(1+\mathrm{e}^{\mathrm{i}k_1d})\right]
\end{cases}\tag{A.13}$$

The system of algebraic equation (A.12) can be easily solved to give analytical expressions for A and $\boldsymbol{B}$. These expressions can be used to obtain the Fourier displacements of the half-space surface in the x-direction and in the z-direction. In accordance with the general representation (A.3) and the solutions (A.12) these displacements read

$$\begin{aligned} u_{\omega,k_1,k_2}(k_1,k_2,0,\omega) &= \left[\mathrm{i}k_1 f + \mathrm{i}k_2 g_z - \frac{\partial g_y}{\partial z}\right]_{z=0} = \mathrm{i}k_1 A + \mathrm{i}k_2 B_z + R_{\mathrm{T}} B_y \\ w_{\omega,k_1,k_2}(k_1,k_2,0,\omega) &= \left[\frac{\partial f}{\partial z} + \mathrm{i}k_1 g_y - \mathrm{i}k_2 g_x\right]_{z=0} = -R_{\mathrm{L}} A + \mathrm{i}k_1 B_y - \mathrm{i}k_2 B_x \end{aligned} \tag{A.14}$$

Substituting expressions for A and $\boldsymbol{B}$ that were obtained from the system (A.12) into Eq. (A.14), one obtains

$$\begin{aligned} u_{\omega,k_1,k_2}(k_1,k_2,0,\omega) &= a_{11} H_x + a_{13} H_z \\ w_{\omega,k_1,k_2}(k_1,k_2,0,\omega) &= a_{31} H_x + a_{33} H_z \end{aligned} \tag{A.15}$$

with

$$\begin{aligned} a_{11} &= \tfrac{1}{R_{\mathrm{T}} \Delta_0}\left[2k_1^2 R_{\mathrm{T}}^2 - \left(R_{\mathrm{T}}^2 + k_2^2\right) q + 4k_2^2 R_{\mathrm{L}} R_{\mathrm{T}}\right] \\ a_{13} &= \tfrac{\mathrm{i}k_1}{\Delta_0}(q - 2R_{\mathrm{L}} R_{\mathrm{T}}), \quad a_{31} = -a_{13}, \quad a_{33} = \tfrac{\omega^2}{c_{\mathrm{T}}^2}\tfrac{R_{\mathrm{L}}}{\Delta_0} \\ q &= k_1^2 + k_2^2 + R_{\mathrm{T}}^2, \qquad \Delta_0 = q^2 - 4\left(k_1^2 + k_2^2\right) R_{\mathrm{L}} R_{\mathrm{T}} \end{aligned} \tag{A.16}$$

Applying the inverse Fourier transform with respect to k_2 to Eq. (A.15) and substituting expressions (A.13), we find

$$\begin{cases} u_{\omega,k_1} = \tfrac{K}{2\pi\tilde{\mu}} I_{11} u_{\omega,k_1} + \tfrac{I_{13}}{2\pi\tilde{\mu}}\left(w_{\omega,k_1}^{\mathrm{beam}} D(\omega,k_1) - 2\pi P \delta(\omega - k_1 V)(1 + \mathrm{e}^{\mathrm{i}k_1 d})\right) \\ w_{\omega,k_1} = \tfrac{K}{2\pi\tilde{\mu}} I_{31} u_{\omega,k_1} + \tfrac{I_{33}}{2\pi\tilde{\mu}}\left(w_{\omega,k_1}^{\mathrm{beam}} D(\omega,k_1) - 2\pi P \delta(\omega - k_1 V)(1 + \mathrm{e}^{\mathrm{i}k_1 d})\right) \end{cases} \tag{A.17}$$

with

$$I_{ij} = \int_{-\infty}^{\infty} a_{ij} \frac{\sin k_2 a}{k_2 a}\, \mathrm{d}k_2.$$

By introducing the following notations

$$\begin{aligned} b_{11}(\omega,k_1) &= \frac{K}{2\pi(\mu - \mathrm{i}\omega\mu^*)} I_{11}(\omega,k_1) - 1, \qquad b_{12}(\omega,k_1) = \frac{I_{13}(\omega,k_1)}{2\pi(\mu - \mathrm{i}\omega\mu^*)} D(\omega,k_1), \\ b_{21}(\omega,k_1) &= -\frac{K}{2\pi(\mu - \mathrm{i}\omega\mu^*)} I_{13}(\omega,k_1), \qquad b_{22} = \frac{I_{33}(\omega,k_1)}{2\pi(\mu - \mathrm{i}\omega\mu^*)} D(\omega,k_1) - 1, \end{aligned}$$

the system of Eq. (A.17) may be rewritten as

$$\begin{aligned} b_{11} u_{\omega,k_1} + b_{12} w_{\omega,k_1} &= \frac{P}{(\mu - \mathrm{i}\omega\mu^*)} I_{13} \delta(\omega - k_1 V)\left(1 + \mathrm{e}^{\mathrm{i}k_1 d}\right) \\ b_{21} u_{\omega,k_1} + b_{22} w_{\omega,k_1} &= \frac{P}{(\mu - \mathrm{i}\omega\mu^*)} I_{33} \delta(\omega - k_1 V)\left(1 + \mathrm{e}^{\mathrm{i}k_1 d}\right). \end{aligned}$$

Solving this system of equations with respect to w_{ω,k_1} and then applying to the obtained expression the inverse Fourier transforms with respect to ω and k_1, one obtains the following final expression for the vertical displacement of the beam

$$
\begin{aligned}
w^{\text{beam}}(x,t) &= \frac{1}{4\pi^2}\int_{-\infty}^{\infty}\int_{-\infty}^{\infty} w^{\text{beam}}_{\omega,k_1}(k_1,\omega)\exp(-\mathrm{i}\omega t+\mathrm{i}k_1 x)\,\mathrm{d}\omega\,\mathrm{d}k_1\\
&= \frac{1}{4\pi^2}\int_{-\infty}^{\infty}\int_{-\infty}^{\infty} w_{\omega,k_1}(k_1,0,0,\omega)\exp(-\mathrm{i}\omega t+\mathrm{i}k_1 x)\,\mathrm{d}\omega\,\mathrm{d}k_1\\
&= \frac{P}{4\pi^2}\int_{-\infty}^{\infty}\int_{-\infty}^{\infty} \frac{\delta(\omega-k_1V)}{(\mu-\mathrm{i}\omega\mu^*)}(1+\exp(\mathrm{i}k_1 d))\frac{b_{11}I_{33}-b_{21}I_{13}}{b_{11}b_{22}-b_{21}b_{12}}\exp(-\mathrm{i}\omega t+\mathrm{i}k_1 x)\,\mathrm{d}\omega\,\mathrm{d}k_1\\
&= \frac{P}{4\pi^2}\int_{-\infty}^{\infty} \frac{1}{(\mu-\mathrm{i}\omega\mu^*)}\frac{b_{11}I_{33}-b_{21}I_{13}}{b_{11}b_{22}-b_{21}b_{12}}\bigg|_{\omega=k_1V}\exp(\mathrm{i}k_1(x-Vt))(1+\exp(\mathrm{i}k_1 d))\,\mathrm{d}k_1
\end{aligned}
$$

Appendix B

Consider the steady-state response of a visco-elastic (due to the Voigt model) half-space to a point harmonic load $P\exp(-\mathrm{i}\omega t)$ that is vertically applied to the half-space surface at $r=0$. To find an expression for the vertical displacement of the half-space surface one may apply a standard approach which is presented, for example, in Achenbach (1973). Using this approach, the following expression is found for the vertical displacement of the half-space surface:

$$
w(r,0,t) = -\frac{P\omega^2\exp(-\mathrm{i}\omega t)}{2\pi(\mu-\mathrm{i}\omega\mu^*)\tilde{c}_{\mathrm{T}}^2}\int_0^{\infty}\xi\beta_{\mathrm{L}}\frac{J_0(\xi r)\,\mathrm{d}\xi}{\left(2\xi^2-\omega^2/\tilde{c}_{\mathrm{T}}^2\right)^2-4\xi^2\beta_{\mathrm{L}}\beta_{\mathrm{T}}} \tag{B.1}
$$

where $w(r,z,t)$ is the vertical half-space displacement, r is the distance from the loading point, $\beta_{\mathrm{L,T}}=\sqrt{\xi^2-\omega^2/\tilde{c}_{\mathrm{L,T}}^2}$, $\tilde{c}_{\mathrm{L}}^2=c_{\mathrm{L}}^2-\mathrm{i}\omega(\lambda^*+2\mu^*)/\rho$, $\tilde{c}_{\mathrm{T}}^2=c_{\mathrm{T}}^2-\mathrm{i}\omega\mu^*/\rho$ and $J_0(\ldots)$ is the Bessel function of the order zero.

The expression (B.1) is the same as presented in Achenbach (1973) for the Laplace image of the transient response of an elastic half-space to the step load, save the following changes:

$$
\mu\to\mu-\mathrm{i}\omega\mu^*,\quad c_{\mathrm{L,T}}^2\to\tilde{c}_{\mathrm{L,T}}^2,\quad p^2\to-\omega^2,\quad P/p\to P,
$$

with p the Laplace transform parameter.

Let us evaluate the integral

$$
I=\int_0^{\infty}\xi\beta_{\mathrm{L}}\frac{J_0(\xi r)\,\mathrm{d}\xi}{\left(2\xi^2-\omega^2/\tilde{c}_{\mathrm{T}}^2\right)^2-4\xi^2\beta_{\mathrm{L}}\beta_{\mathrm{T}}} \tag{B.2}
$$

that, in accordance with Eq. (B.1), determines the spatial variation of $w(r,0,t)$. The evaluation will be performed by employing the contour integration technique (Fuchs et al., 1964). Assuming that the damping in the half-space is small, that is $\mu^*/\mu\ll 1/\omega$, the square roots β_{L} and β_{T} may be approximated as

$$
\begin{aligned}
\beta_{\mathrm{L}} &= \sqrt{\xi^2-\frac{\omega^2}{\tilde{c}_{\mathrm{L}}^2}}=\sqrt{\xi^2-\frac{\omega^2}{c_{\mathrm{L}}^2-\mathrm{i}\omega(\lambda^*+2\mu^*)/\rho}}\approx\sqrt{\xi^2-\frac{\omega^2}{c_{\mathrm{L}}^2}\left(1+\frac{\mathrm{i}\omega(\lambda^*+2\mu^*)}{\rho c_{\mathrm{L}}^2}\right)},\\
\beta_{\mathrm{T}} &= \sqrt{\xi^2-\frac{\omega^2}{\tilde{c}_{\mathrm{T}}^2}}=\sqrt{\xi^2-\frac{\omega^2}{c_{\mathrm{T}}^2-\mathrm{i}\omega\mu^*/\rho}}\approx\sqrt{\xi^2-\frac{\omega^2}{c_{\mathrm{T}}^2}\left(1+\frac{\mathrm{i}\omega\mu^*}{\mu}\right)}.
\end{aligned} \tag{B.3}
$$

Accordingly, the branch points of the integrand in Eq. (B.2) are given as

$$
\xi_{\mathrm{L}}^{\pm}\approx\pm\frac{\omega}{c_{\mathrm{L}}}\left(1+\frac{\mathrm{i}\omega(\lambda^*+2\mu^*)}{2\rho c_{\mathrm{L}}^2}\right),\qquad \xi_{\mathrm{T}}^{\pm}\approx\pm\frac{\omega}{c_{\mathrm{T}}}\left(1+\frac{\mathrm{i}\omega\mu^*}{2\mu}\right). \tag{B.4}
$$

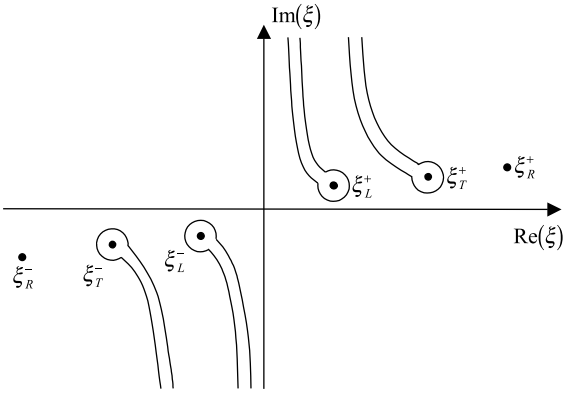

Fig. 6. Poles, branch points and branch cuts in the complex ξ-plane.

Additionally, it may be shown that if λ^* and μ^* are proportional with the same proportionality coefficient as λ and μ, then the poles of the integrand in Eq. (B.2) read

$$\xi_{\mathrm{R}}^{\pm} = \pm\frac{\omega}{\tilde{c}_{\mathrm{R}}} \approx \pm\frac{\omega}{c_{\mathrm{R}}}\frac{c_{\mathrm{T}}}{\tilde{c}_{\mathrm{T}}} = \pm\frac{\omega}{c_{\mathrm{R}}}\frac{1}{\sqrt{1-\mathrm{i}\omega\mu^*/\mu}} \approx \pm\frac{\omega}{c_{\mathrm{R}}}\left(1+\frac{\mathrm{i}\omega\mu^*}{2\mu}\right) \tag{B.5}$$

with c_{R} the Rayleigh wave velocity.

Thus, the integrand in Eq. (B.2) has six singular points – two poles given by Eq. (B.5) and four branch points given by Eq. (B.4). The position of these singular points in the complex ξ – plane together with the branch cuts that ensure positive sign of the radicals all over the complex plane are shown in Fig. 6.

To perform the contour integration we use the following integral representation of the Bessel function (Abramowitz and Stegun, 1970):

$$J_0(\xi r) = \frac{1}{\pi\mathrm{i}}\int_1^{\infty}\frac{\mathrm{e}^{\mathrm{i}\xi rs}-\mathrm{e}^{-\mathrm{i}\xi rs}}{\sqrt{s^2-1}}\,\mathrm{d}s. \tag{B.6}$$

Substitution of Eq. (B.6) into Eq. (B.2) yields

$$I = \frac{1}{\pi\mathrm{i}}\int_0^{\infty}\int_1^{\infty}\xi\beta_{\mathrm{L}}\frac{\exp(\mathrm{i}\xi rs)-\exp(-\mathrm{i}\xi rs)}{D_{\mathrm{H}}\sqrt{s^2-1}}\,\mathrm{d}\xi\,\mathrm{d}s = \int_1^{\infty}\frac{I_1-I_2}{\sqrt{s^2-1}}\,\mathrm{d}s \tag{B.7}$$

with

$$I_1 = \frac{1}{\pi\mathrm{i}}\int_0^{\infty}\xi\beta_{\mathrm{L}}\frac{\exp(+\mathrm{i}\xi rs)}{D_{\mathrm{H}}}\,\mathrm{d}\xi, \quad I_2 = \frac{1}{\pi\mathrm{i}}\int_0^{\infty}\xi\beta_{\mathrm{L}}\frac{\exp(-\mathrm{i}\xi rs)}{D_{\mathrm{H}}}\,\mathrm{d}\xi,$$
$$D_H = \left(2\xi^2-\omega^2/\tilde{c}_{\mathrm{T}}^2\right)^2 - 4\xi^2\beta_{\mathrm{L}}\beta_{\mathrm{T}}.$$

To evaluate the integral I_1, we close the contour of integration over the first quadrant ($\mathrm{Re}(\xi)>0$, $\mathrm{Im}(\xi)>0$) of the complex ξ-plane, see Fig. 7a. In accordance with the residue theorem, the integral along this closed contour is equal to the residue of the integrand taken in the point $\xi=\xi_{\mathrm{R}}^+$ and multiplied by $2\pi\mathrm{i}$:

$$\frac{1}{\pi\mathrm{i}}\oint\xi\beta_{\mathrm{L}}\frac{\exp(+\mathrm{i}\xi rs)}{D_{\mathrm{H}}}\,\mathrm{d}\xi = 2\left(\frac{\xi\beta_{\mathrm{L}}\exp(+\mathrm{i}\xi rs)}{\partial D_{\mathrm{H}}/\partial\xi}\right)_{\xi=\xi_{\mathrm{R}}^+}. \tag{B.8}$$

Taken into account that the integral over the large quarter-circle vanishes (according to the Jordan's lemma) as the radius of this circle tends to infinity, and neglecting the contribution of integration around

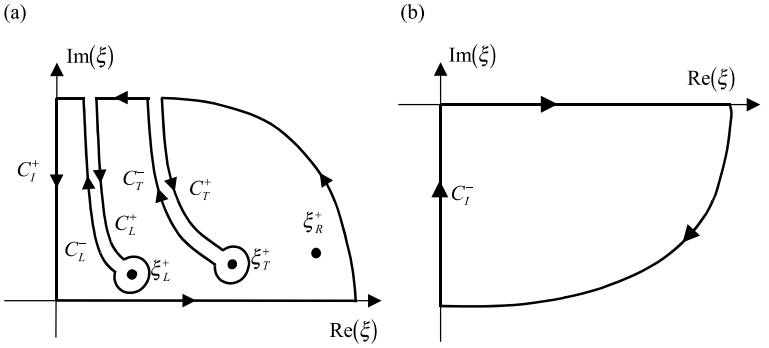

Fig. 7. Integration contours for I_1 and I_2.

the branch points that vanishes also as the radius of the circles surrounding these points tends to zero, one may rewrite (B.8) as

$$I_1+\frac{1}{\pi \mathrm{i}}\left(\int_{C_\mathrm{T}^+}+\int_{C_\mathrm{T}^-}+\int_{C_\mathrm{L}^+}+\int_{C_\mathrm{L}^-}+\int_{C_\mathrm{I}^+}\right)\xi\beta_\mathrm{L}\frac{\exp(+\mathrm{i}\xi rs)}{D_\mathrm{H}}\,\mathrm{d}\xi=2\left(\frac{\xi\beta_\mathrm{L}\exp(+\mathrm{i}\xi rs)}{\partial D_\mathrm{H}/\partial\xi}\right)_{\xi=\xi_\mathrm{R}^+}. \tag{B.9}$$

To evaluate I_2 we close the contour over the fourth quadrant ($\mathrm{Re}(\xi)>0$, $\mathrm{Im}(\xi)<0$) of the complex ξ-plane, see Fig. 7b. Since there are no poles inside this contour and the integral over the large quarter-circle vanishes, the following equality is valid

$$I_2+\frac{1}{\pi \mathrm{i}}\int_{C_\mathrm{I}^-}\xi\beta_\mathrm{L}\frac{\exp(-\mathrm{i}\xi rs)}{D_\mathrm{H}}\,\mathrm{d}\xi=0. \tag{B.10}$$

Subtracting Eq. (B.10) from Eq. (B.9) and taking into account that $\int_{C_\mathrm{I}^+}(\ldots)\,\mathrm{d}\xi=\int_{C_\mathrm{I}^-}(\ldots)\,\mathrm{d}\xi$, we obtain

$$I_1-I_2=2\left(\frac{\xi\beta_\mathrm{L}\exp(+\mathrm{i}\xi rs)}{\partial D_\mathrm{H}/\partial\xi}\right)_{\xi=\xi_\mathrm{R}^+}-\frac{1}{\pi \mathrm{i}}\left(\int_{C_\mathrm{T}^+}+\int_{C_\mathrm{T}^-}+\int_{C_\mathrm{L}^+}+\int_{C_\mathrm{L}^-}\right)\xi\beta_\mathrm{L}\frac{\exp(+\mathrm{i}\xi rs)}{D_\mathrm{H}}\,\mathrm{d}\xi. \tag{B.11}$$

It may be shown that the contribution of the second term in the expression (B.11) decreases with the distance r much faster then the contribution of the first term. The physical background of this fact is that the first term in Eq. (B.11) describes the Rayleigh wave that decays as $1/\sqrt{r}$ (in the elastic case), while the second term is related to the body waves that decay proportionally to $1/r$. Thus, at a large distance from the load, it is possible to approximate the difference I_1-I_2 by accounting for the first term in Eq. (B.11), i.e. by considering the contribution of the Rayleigh wave only. This yields

$$I=\int_1^\infty\frac{I_1-I_2}{\sqrt{s^2-1}}\,\mathrm{d}s=2\left(\frac{\xi\beta_\mathrm{L}}{\partial D_\mathrm{H}/\partial\xi}\right)_{\xi=\xi_\mathrm{R}^+}\int_1^\infty\frac{\exp(+\mathrm{i}\xi_\mathrm{R}^+rs)}{\sqrt{s^2-1}}\,\mathrm{d}s. \tag{B.12}$$

By employing the following integral representation of the Hankel function

$$H_0^{(1)}(r)=\frac{2}{\mathrm{i}\pi}\int_1^\infty\frac{\exp(\mathrm{i}rs)}{\sqrt{s^2-1}}\,\mathrm{d}s,$$

we may rewrite Eq. (B.12) as

$$I=\pi\mathrm{i}\left(\frac{\xi\beta_\mathrm{L}}{\partial D_\mathrm{H}/\partial\xi}\right)_{\xi=\xi_\mathrm{R}^+}H_0^{(1)}\left(\xi_\mathrm{R}^+r\right). \tag{B.13}$$

At a large distance from the load, i.e. for $r \gg c_R/\omega$, one may use the following asymptotic form of the Hankel function (Abramowitz and Stegun, 1970):

$$H_0^{(1)}(\xi_R^+ r)\Big|_{r\gg c_R/\omega} \approx \sqrt{\frac{2}{\pi\xi_R^+ r}}\exp\left(i\left(\xi_R^+ r - \frac{\pi}{4}\right)\right). \tag{B.14}$$

Thus, substituting Eq. (B.13) into Eq. (B.1) and accounting for the asymptotic form (B.14) and for the expression for ξ_R^+ (B.5), we obtain

$$w(r,0,t)|_{r\gg c_R/\omega} = -\frac{P i\omega^2 \exp(-i\omega t)}{2(\mu - i\omega\mu^*)\tilde{c}_T^2}\left(\frac{\xi\beta_L}{\partial D_H/\partial\xi}\right)_{\xi=\xi_R^+}\sqrt{\frac{2}{\pi\xi_R^+ r}}\exp\left(i\left(\frac{\omega r}{c_R}\left(1+\frac{i\omega\mu^*}{2\mu}\right)-\frac{\pi}{4}\right)\right). \tag{B.15}$$

Accordingly, the absolute value of $w(r,0,t)|_{r\gg c_R/\omega}$ is given as

$$|w(r,0,t)|_{r\gg c_R/\omega} = \frac{A}{\sqrt{r}}\exp\left(-\frac{\omega^2}{2c_R}\frac{\mu^*}{\mu}r\right)$$

with

$$A = \frac{P\omega^2}{\sqrt{2\pi}}\left|\frac{1}{(\mu - i\omega\mu^*)\tilde{c}_T^2\sqrt{\xi_R^+}}\left(\frac{\xi\beta_L}{\partial D_H/\partial\xi}\right)_{\xi=\xi_R^+}\right|.$$

References

Abramowitz, M., Stegun, I.A., 1970. Handbook of mathematical functions; with formulas, graphs, and mathematical tables. Dover, New York.

Achenbach, J.D., 1973. Wave propagation in elastic solids. NHPC, Amsterdam-London.

Al-Hundaidi, M.O., Chen, P.A., Rainer, J.H., Tremblay, M., 1996. Shear moduli and damping in frozen and unfrozen clay by resonant column tests. Canadian Geotechnical J. 33 (3), 510–514.

Dieterman, H.A., Metrikine, A.V., 1997. Steady-state displacements of a beam on an elastic half-space due to a uniformly moving constant load. Eur. J. Mech. A/Solids 16 (2), 295–306.

Filippov, A.P., 1961. Steady-state vibrations of an infinite beam on elastic half-space subjected to a moving load. Izvestija AN SSSR OTN Mehanika i Mashinostroenie 6, 97–105.

Fuchs, B.A., Shabat, B.V., Berry, J., 1964. Functions of Complex Variables and Some of Their Applications. Oxford, Pergamon.

Grundmann, H., Lieb, M., Trommer, E., 1999. The response of a layered half-space to traffic loads moving along its surface. Arch. Appl. Mech. 69 (1), 55–67.

Hopkins, T., Silva, J.P., Marder, B., Turban, B., Kelley, B., 1999. Maglift Monorail: a high performance, low cost, and low risk solution for high-speed transportation, Proceedings of High Speed Ground Transportation Association Annual Conference, Seatle, June 6–9.

Kim, D.S., Lee, J.S., 1998. Source and attenuation characteristics of various ground vibrations. Geotechnical Special Publication (2), ASCE, Reston, VA, USA, pp. 1507–1517.

Krylov, V.V., 1995. Generation of ground vibrations by superfast trains. Appl. Acoust. 44 (2), 149–164.

Labra, J.J., 1975. An axially stressed railroad track on an elastic continuum subjected to a moving load. Acta Mechanica 22, 113–129.

Lansing, D.L., 1966. The displacements in an elastic half-space due to a moving concentrated normal load. NASA technical report, TR R-238.

Metrikine, A.V., Dieterman, H.A., 1997. Three-dimensional vibrations of a beam on an elastic half-space: resonance interaction of vertical-longitudinal and lateral beam waves. Trans. ASME J. Appl. Mech. 64, 951–956.

Metrikine, A.V., Popp, K., 1999. Vibration of a periodically supported beam on an elastic half-space. Eur. J. Mech. A/Solids 18 (4), 679–701.

Miklowitz, J., 1978. The theory of elastic waves and waveguides. NHPC, Amsterdam.

Popp, K., Kruse, H., Kaiser, I., 1999. Vehicle-track dynamics in the mid-frequency range. Vehicle Syst. Dyn. 31 (5–6), 423–464.

Sheng, X., Jones, C.J.C., Petyt, M., 1999. Ground vibration generated by a load moving along a railway track. J. Sound Vibration 228 (1), 129–156.

Vesnitskii, A.I., Metrikine, A.V., 1996. Transition radiation in mechanics. Physics – Uspekhi 39 (10), 983–1007.